HOKKAIDO UNIVERSITY

Title	Station-Orientation Catalog for Australian Broadband Seismic Stations
Author(s)	Tarumi, Kotaro; Yoshizawa, Kazunori
Citation	Pure and applied geophysics https://doi.org/10.1007/s00024-025-03827-7
Issue Date	2025-09-16
Doc URL	https://hdl.handle.net/2115/98110
Rights	This version of the article has been accepted for publication, after peer review (when applicable) and is subject to Springer Nature's AM terms of use, but is not the Version of Record and does not reflect post-acceptance improvements, or any corrections. The Version of Record is available online at: https://doi.org/10.1007/s00024-025-03827-7
Type	journal article
File Information	Tarumi_and_Yoshizawa2025PAGEOPH.pdf

Hokkaido University Collection of Scholarly and Academic Papers : HUSCAP

Pure Appl. Geophys.
© 2025 The Author(s), under exclusive licence to Springer Nature Switzerland AG
https://doi.org/10.1007/s00024-025-03827-7

Pure and Applied Geophysics

Station-Orientation Catalog for Australian Broadband Seismic Stations

Kotaro Tarumi[1,2] and Kazunori Yoshizawa[1,2]

Abstract—Many broadband seismic stations deployed permanently and temporarily in the Australian continent have been used for various seismological investigations in and around Australia. Although two horizontal components are generally assumed to be oriented in the north and east directions, as reported by data providers, misorientations of horizontal components from the true geographic north direction cannot be avoided in practical field observations, even at well-maintained permanent stations. In this paper, we applied a polarization analysis to almost all stations in Australia to estimate the misorientations of horizontal components using long-period teleseismic P-waves. A large data set of P-wave arrival angles allows us to successfully detect probable horizontal misorientations, including significant temporal changes in some stations, which generally coincide with reported equipment replacements included in the EarthScope (IRIS) catalog. However, we also detected some unreported temporal changes in station orientation that may result from undocumented maintenance activities, such as sensor reorientation, which are typically not reflected in metadata. Improper corrections for orientation may affect waveform-based studies for the Earth's internal exploration, as demonstrated by teleseismic receiver function analyses, especially in the transverse component. Compiling the information on such time-dependent misorientations, we created a full catalog of horizontal-component orientations for both permanent and temporary stations in Australia, which is widely available for the community.

Keywords: Australia, seismometer misorientation, P-wave polarization, receiver function.

1. Introduction

A large number of broadband seismic stations deployed permanently or temporarily in the Australian continent have provided key information on seismic wave propagation (e.g., Kennett & Furumura, 2008), seismic sources (e.g., Hejrani & Tkalcic, 2020), and seismic structure (e.g., Birkey & Ford, 2023; Eakin et al., 2023; Kennett et al., 2013; Yoshizawa, 2014) in and around Australia. As an initial step for the three-component seismic waveform analysis, we generally rotate two horizontal components (e.g., NS/EW) to radial and transverse directions, supposing that the horizontal sensors are oriented in the north and east (or in reported) directions. However, as several earlier studies suggested, there is a possibility of nontrivial misorientation of horizontal components at some stations (e.g., Laske, 1995; Schulte-Pelkum et al., 2001; Yoshizawa et al., 1999). Also, temporal changes in the amplitude gain of seismometers may occur at some permanent stations over a long observation period (Ekström et al., 2006). Such errors or uncertainties in the documented catalog values, particularly the ambiguities in the horizontal-component orientation, would prevent us from performing precise waveform analyses that depend on the horizontal directions, such as shear-wave splitting measurements, Love-wave dispersion analysis, and the azimuthal dependency of receiver functions.

The horizontal orientation of seismic stations can be estimated by measuring the arrival angles of teleseismic P waves (e.g., Albuquerque et al., 2024; Deng et al., 2024; Schulte-Pelkum et al., 2001; Yoshizawa et al., 1999) or Rayleigh waves (e.g., Ekström & Busby, 2008; Larson & Ekström, 2002; Laske & Masters, 1996) at longer periods for a large number of seismic events. Zha et al. (2013) developed the method for determining the horizontal orientation of ocean bottom seismometers based on the vertical-radial cross correlation of Rayleigh-wave polarization from ambient noise data. More recently,

Supplementary Information The online version contains supplementary material available at https://doi.org/10.1007/s00024-025-03827-7.

[1] Department of Natural History Sciences, Graduate School of Science, Hokkaido University, Sapporo 0600810, Japan. E-mail: tarumi.kotaro.jp@gmail.com; yoshizawa@sci.hokudai.ac.jp

[2] Department of Earth and Planetary Sciences, Faculty of Science, Hokkaido University, Sapporo 0600810, Japan.

Published online: 16 September 2025

Sun et al. (2024) developed an alternative method for measuring station orientation using the azimuthal dependence of receiver function amplitudes for the direct P-phase.

Rayleigh waves generally oscillate elliptically in the radial-vertical plane, but their particle motions become more complicated in heterogeneous and anisotropic media (Crampin, 1975). Moreover, due to the dispersive nature of surface waves, the arrival-angle anomalies (or deviations from the great-circle path) depend significantly on the frequency (Laske, 1995; Yoshizawa et al., 1999), which may increase uncertainties in the estimated station orientation. Furthermore, the overlaps by preceding Love waves in the transverse component make it difficult to perform arrival-angle analysis of Rayleigh waves at relatively shorter epicentral distances of less than 50° (Yoshizawa et al., 1999). On the contrary, the onset of teleseismic P-waves exhibits a relatively simple linear motion in the radial-vertical plane without frequency dependence. Teleseismic P waves with the near-vertical incidence to the station mainly sample the lower mantle where lateral heterogeneities are weak. Thus, the ray-bending effects on P-waves due to strong lateral heterogeneity in the upper mantle can be milder than that on surface waves (Yoshizawa et al., 1999), in addition to the relatively smaller influence from anisotropy on P-waves compared to surface waves (Crampin et al., 1982).

Recently, major seismological data centers, such as EarthScope (formerly IRIS: Incorporated Research Institutions for Seismology), have provided us with more precise information on the station orientation for their affiliated stations worldwide, including Australian stations. Given proper information from careful calibrations, many of the broadband horizontal channels in major stations in global networks (such as the Global Seismograph Network) have been named BH1 and BH2 (for the first and second components) rather than conventional BHN and BHE (North and East), when the true horizontal directions deviate from the geographic north and east (Ekström & Busby, 2008). Ekström (2008) has also provided practically useful tables on the station orientation for GSN stations until 2015. However, a number of seismic stations from local data providers and temporary seismic networks, including transportable seismic arrays (e.g., SKIPPY in Australia; Hilst et al., 1994), still lack precise information on horizontal orientations, which is crucial for researchers wishing to utilize these valuable waveform data sets.

In this paper, we collect a large number of P-wave arrival angle data to estimate the horizontal orientation of many broadband seismic stations in Australia, modeled on the method of polarization analysis by Vidale (1986) utilized in earlier study by Yoshizawa et al. (1999). Through the polarization analysis of teleseismic P-wave particle motions, we construct a complete catalog of the horizontal orientation of currently available broadband stations in Australia, which can be used for a variety of future applications of seismic data analyses with horizontal components.

2. Data and Method

2.1. Data

We used the three-component teleseismic P-wave data downloaded from the EarthScope Data Management Center (EarthScope DMC) and Australian Passive Seismic Server (AusPass) for 4004 seismic events with moment magnitude Mw $\geq$ 5.5 from 1987 to 2019. Our dataset includes both permanent and temporary broadband stations shown in Fig. 1a, b. Permanent seismic networks include IRIS/IDA (red triangles in Fig. 1a; Network II, Scripps Institution of Oceanography, 1986), IRIS/USGS (purple triangles in Fig. 1a; Network IU, Albuquerque Seismological Laboratory/USGS, 1988), GEOSCOPE (green triangles in Fig. 1a; Network G, Institut de physique du globe de Paris (IPGP) and École et Observatoire des Sciences de la Terre de Strasbourg (EOST), 1982), GeoScience Australia (blue triangles in Fig. 1a; Network AU, Geoscience Australia, 2021), and Australian Seismometers in Schools program (orange triangles in Fig. 1a; Network S1, Salmon et al., Salmon et al. (2011)). Temporary stations shown in Fig. 1b involve many temporary seismic arrays, SKIPPY (7B) (Hilst & Kennett, 1993), KIMBA (7D and 7E) (Kennett, 1997, 1998), QUOLL (7F) (Kennett et al., 1999), West Australia

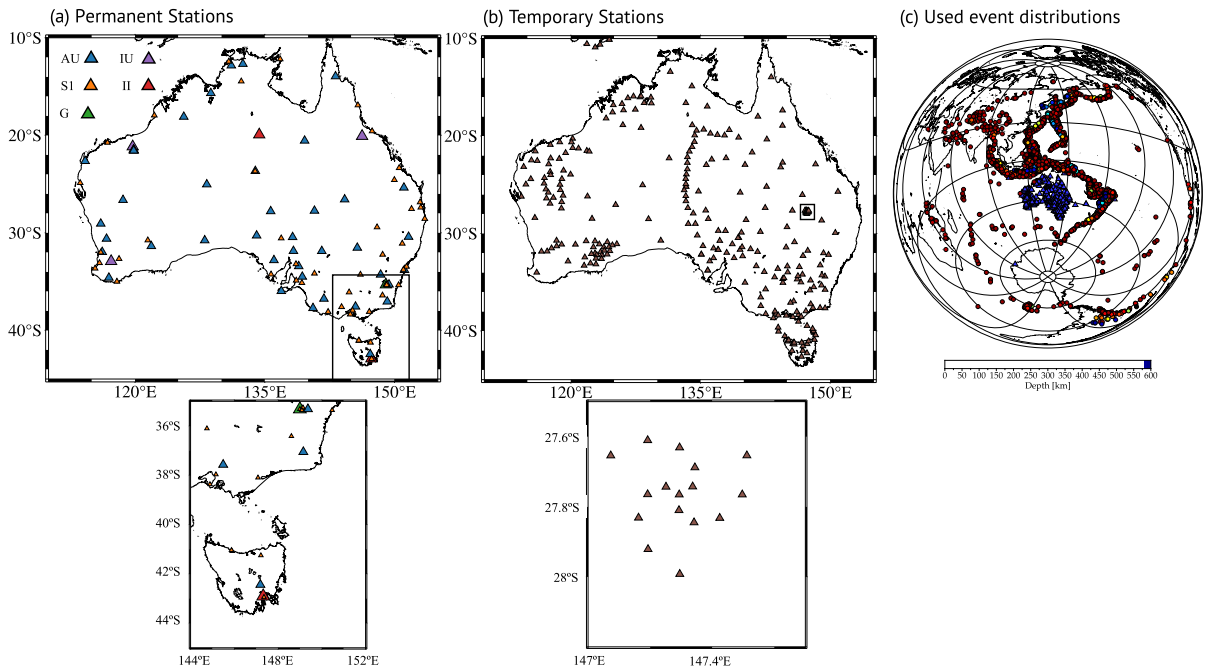


Figure 1

Broadband seismic stations and seismic events used in this study. **a** Permanent stations, with colors indicating different networks (AU, S1, IU, II, and G). **b** Temporary stations. **c** Seismic events used in this study, with colors representing source depths. Blue triangles are employed stations in **a** and **b**. For **a** and **b**, magnified figures for the encompassed areas by rectangles are displayed below each panel

Cratons (7G) (Kennet, 2000), TRIGGER BB (7H) (Rawlinson & Kennett, 2001), TASMAL (7I) (Kennett, 2003), CARPA—Linkage (7J) (Reading & Kennett, 2005), SOC—Southern Craton (7K) (Fontaine & Kennet, 2007), BILBY (6F) (Rawlinson & Kennet, 2008), Bass Strait (1P) (Reading & Rawlinson, 2011), Southern Queensland Spiral Array (SQSPA; 1E) (Tkalcic et al., 2013b), Albany-Fraser Experiment (1K) (Tkalcic et al., 2013a), and Transitions in the Banda Arc-Australia continental collision (1G) (Miller, 2014).

2.2. *Method of P-wave Polarization Analysis*

We employed the complex time-domain polarization analysis of Vidale (1986) to measure P-wave arrival angles from three-component direct P-wave seismograms. This method has been widely used for the polarization analysis of various seismic phases, including an earlier study on misorientation corrections (e.g., Yoshizawa et al., 1999).

First, we converted the time-series waveforms into analytic signals to construct the covariance matrix of the three-component seismograms, with the covariance averaged over 1 s. We then computed the eigenvalues and corresponding eigenvectors of the covariance matrix and solved the minimization problem associated with the inverse of equation (4) in Vidale (1986). This procedure was applied from 80 s before to 60 s after the P-wave arrival, and yielded estimates of the arrival angle, ellipticity (or linearity), and incident angle of the direct P-waves. Details of practical data processing based on this polarization analysis are summarized in the next subsection.

2.3. *Data Processing*

We selected seismic events with Mw $\geq$ 5.5, distance ranges between 30° and 90°, and normalized amplitude of P-wave radiation $> |0.3|$ estimated from the Global CMT catalog (Dziewonski et al., 1981; Ekström et al., 2012). We first corrected the instrument response, converted the waveform data

into the displacement, and applied a bandpass filter between 0.03 and 0.1 Hz. Second, we rotated the two horizontal waveforms into the radial and transverse components based on the station catalog information of horizontal orientation provided by EarthScope DMC and AusPass. To discard the low-quality data, we calculated signal-to-noise ratios (SNR) in the vertical and radial components and removed data with vertical SNR < 5.0 and radial SNR < 3.0. Then, for each seismic event and station, we performed a time-domain complex polarization analysis of Vidale (1986) to measure the horizontal arrival angles Θ of direct P-waves in a similar way to Yoshizawa et al. (1999), which is summarized in Fig. 2. Since teleseismic P-wave typically exhibit linear particle motion in the radial-vertical plane, we applied a data selection criterion requiring the ellipticity parameter P_E to be smaller than 0.175, which was determined empirically. Third, we calculated the median of the time-dependent arrival angles for each event (an orange line in the third panel in Fig. 2a) in a selected time window. In this study, we set the time window as 7.5 s before and after the main P-wave pulse (Fig. 2a). Consequently, in the final step, we compiled a large number of arrival angle data from many seismic events to evaluate the misorientation of horizontal sensors.

Finally, in this study, we adopted the median as a representative measure of arrival-angle anomalies (i.e., deviations from the great-circle direction) over

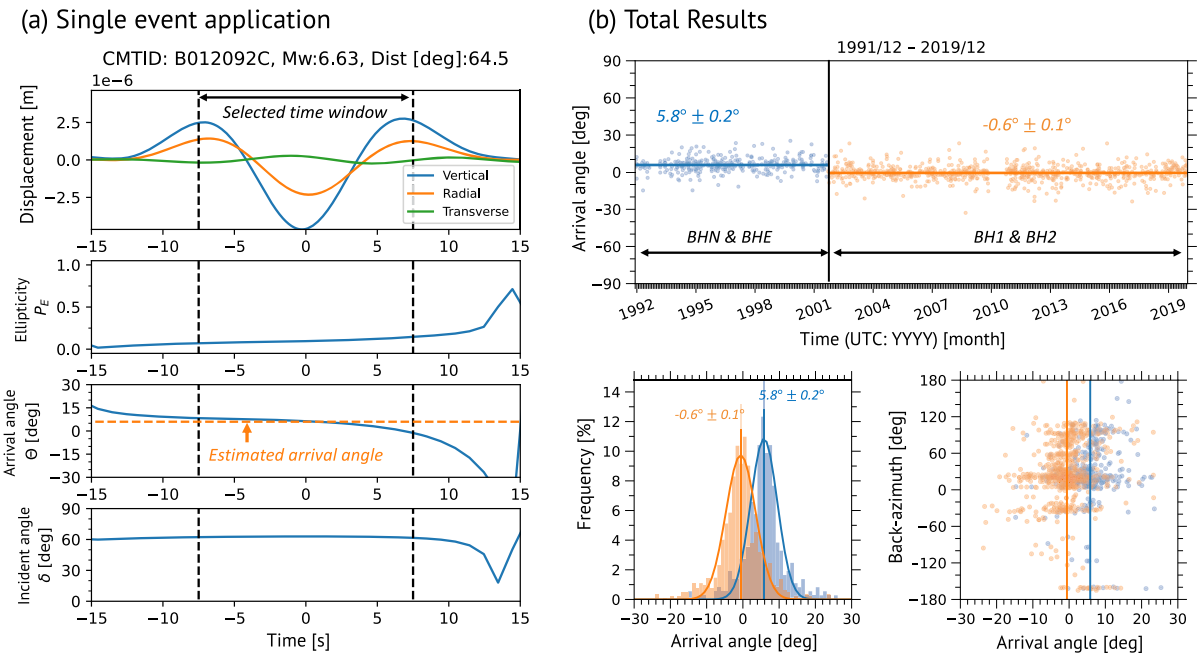


Figure 2

A visual summary of P-wave polarization analysis for IU.NWAO. **a** An example of teleseismic P-wave for an event at the epicentral distance of 64.5° and the estimated polarization parameters. From top to bottom: three-component displacement waveforms rotated to the catalog values of EarthScope metadata (blue: vertical; orange: radial; green: transverse), ellipticity P_E, arrival angle Θ on a horizontal plane, and incident angle δ for the P-wave particle motion. The arrival angle is measured clockwise from the radial (great-circle) direction so that a positive deviation indicates the arrival-angle anomaly to the east. In the third panel, a dashed orange line exhibits a median value in the selected time window encompassed by vertical dashed lines. **b** Compiled P-wave polarization data for all events used for the NWAO station. The top panel represents the time series of P-wave arrival angles. The colors for dots and lines represent the distinct period characterized by different trends of arrival angles. The timing of the arrival-angle trend change in September 2001 (indicated by a solid vertical line) matched well with the reported (i.e., included in the EarthScope catalog) correction of horizontal components by EarthScope. The bottom-left panel shows histograms and fitted Gaussian functions for each period, and the bottom-right one indicates the back-azimuth dependence of the measured arrival angles for all employed events. In the top and bottom-left panels, the estimated station orientations and standard errors are labeled. The colors of the characters correspond to each distinct time period

the selected observation period (Fig. 2b). The distribution of earthquakes around Australia for teleseismic P-wave analysis is concentrated primarily in the north and east (Fig. 1c). This back-azimuthal bias can unintentionally affect the sensor orientation estimates when using the arithmetic mean, as events from dominant directions may bias the result. To mitigate this issue, we adopted the median, which is less sensitive to uneven azimuthal distributions and provides a more robust estimate of central tendency. Nevertheless, we also included the mean values in our catalog (Tables S1–S3 and Tarumi & Yoshizawa, 2024) for comparison. This final step was applied to stations with more than 5 arrival-angle measurements, and several stations with large uncertainties in the time-dependent polarization data were excluded based on visual inspection. The resulting distribution of all events used in this study is shown in Fig. 1c.

Station metadata (or catalog information of horizontal orientation provided by EarthScope) for permanent stations is subject to change from time to time, reflecting irregular maintenance, calibrations, and replacement of instruments. For the permanent stations with a long observation period, we visually inspected the timing of sudden changes in the trend of estimated horizontal misorientation, allowing us to detect some temporal changes at unreported (i.e., not included in the EarthScope catalog) timings (e.g., AU.COEN in Fig. 3f). For the estimation of horizontal misorientation, we divide the period windows in which the median of measured arrival angles is computed, depending on each station, as shown in Figs. 2b and 3.

3. Results

Our arrival-angle measurements enabled us to detect probable misorientations from the geographic north for permanent and temporary stations (Figs. 2, 3, 4, 5, and Fig. S7). All results are summarized in Supplementary Materials 2 (Tables S1–S3) and Zenodo Repository (Tarumi & Yoshizawa, 2024). In this section, we explain our results on the permanent and temporary stations separately.

3.1. Permanent Stations

Figure 2 shows the summary of P-wave polarization measurements for IU.NWAO which has been a long-running station located in southeast Australia since 1992. According to the EarthScope metadata catalog, the channel name of the horizontal components was changed from BHN/BHE to BH1/BH2 in September 2001. Our measured P-wave arrival angles show apparent temporal changes in the polarization trend at this time. The misorientation angle of horizontal sensors was estimated to be about 5.8° before September 2001, and it has decreased to 0.6° since then (by 2019, at least), indicating the improvement in the catalog information of this station.

Note that, for this station, Laske and Masters (1996), Yoshizawa et al. (1999), and Schulte-Pelkum et al. (2001), who employed the particle motion of either Rayleigh wave or teleseismic P-wave before 2000, have already estimated the misalignment from the north by around 5°. In particular, our estimated misorientation angle (5.8°) before September 2001 in Fig. 2b is very close to the estimated value by Schulte-Pelkum et al. (2001), who employed the P wave data in the same period. Fontaine et al. (2009) also used similar P-wave datasets and identified a misalignment of 5°, which is consistent with our results. For the other GSN stations used in this study, our estimated orientations are generally in agreement with the earlier online report (Ekström, 2008).

In addition to temporal changes, we can also see a back-azimuthal dependence in the arrival-angle data (Fig. 2b, bottom-right panel). Such azimuthal variations of arrival angles can also be observed at other stations, which may be worth further investigation in the future, since they may reflect lateral variations in heterogeneity and azimuthal anisotropy, including dipping interfaces, in the upper mantle beneath the seismic station (Fontaine et al., 2009; Schulte-Pelkum et al., 2001). Additionally, when the event distribution does not cover the full azimuthal range, such a back-azimuthal dependence can unintentionally bias the arithmetic mean of arrival angles. Therefore, our choice of the median should effectively suppress such unfavorable weighting.

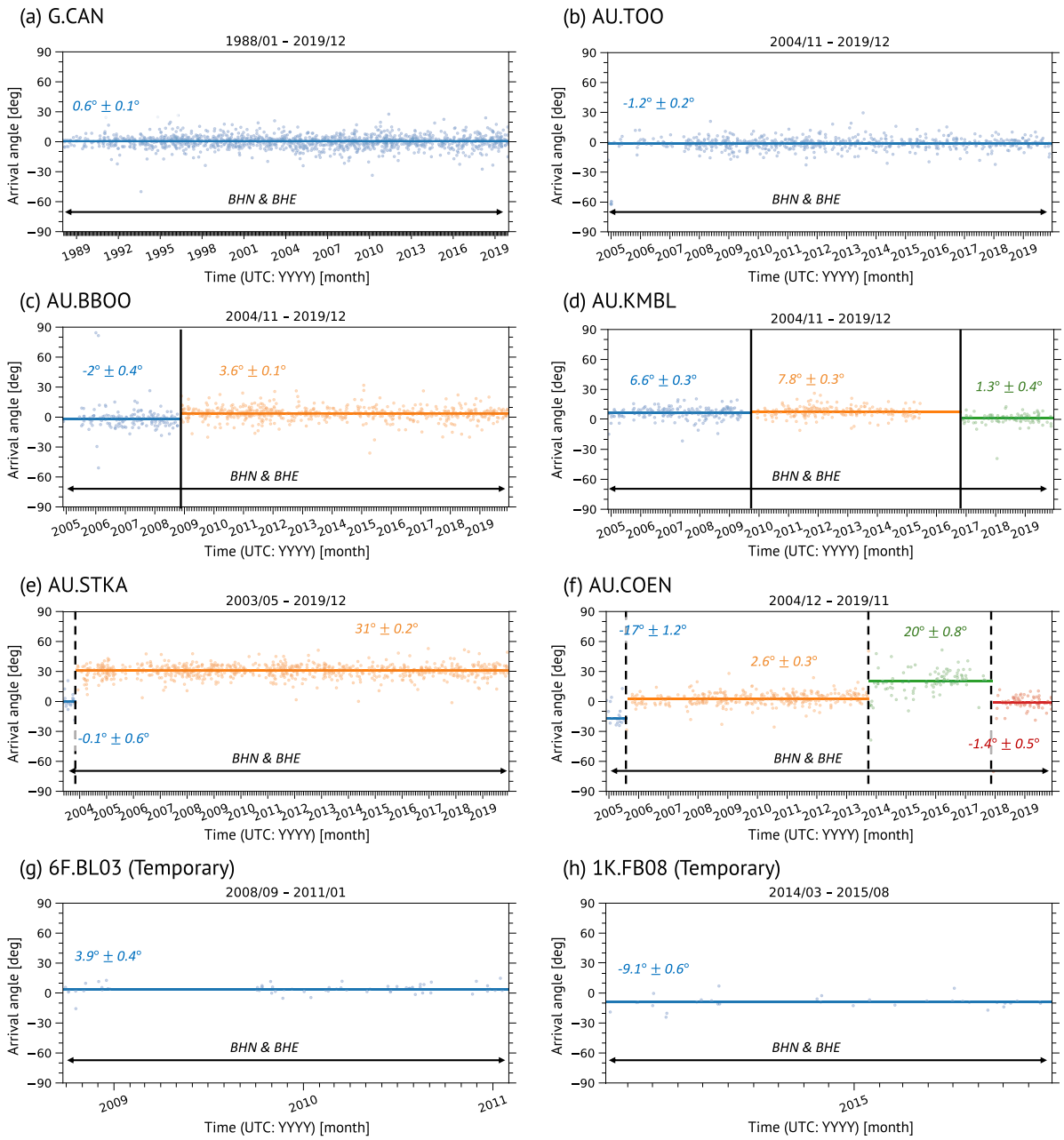


Figure 3

Time-dependent P-wave polarization data (arrival-angle deviation from the great circle) for selected stations, **a–f** permanent stations installed and maintained by GEOSCOPE (G) and Geoscience Australia (AU), and **g**, **h** temporary stations. Notations in these figures are the same as 2b, top panel. The vertical black lines represent the timing of significant trend changes in P-wave arrival angles. Solid vertical lines indicate the timing of the reported maintenance and/or replacement of instruments, and dashed vertical lines represent unknown temporal changes at unreported timings (i.e., not documented in the EarthScope catalog). As described in the main text, no temporal changes were identified for temporary stations

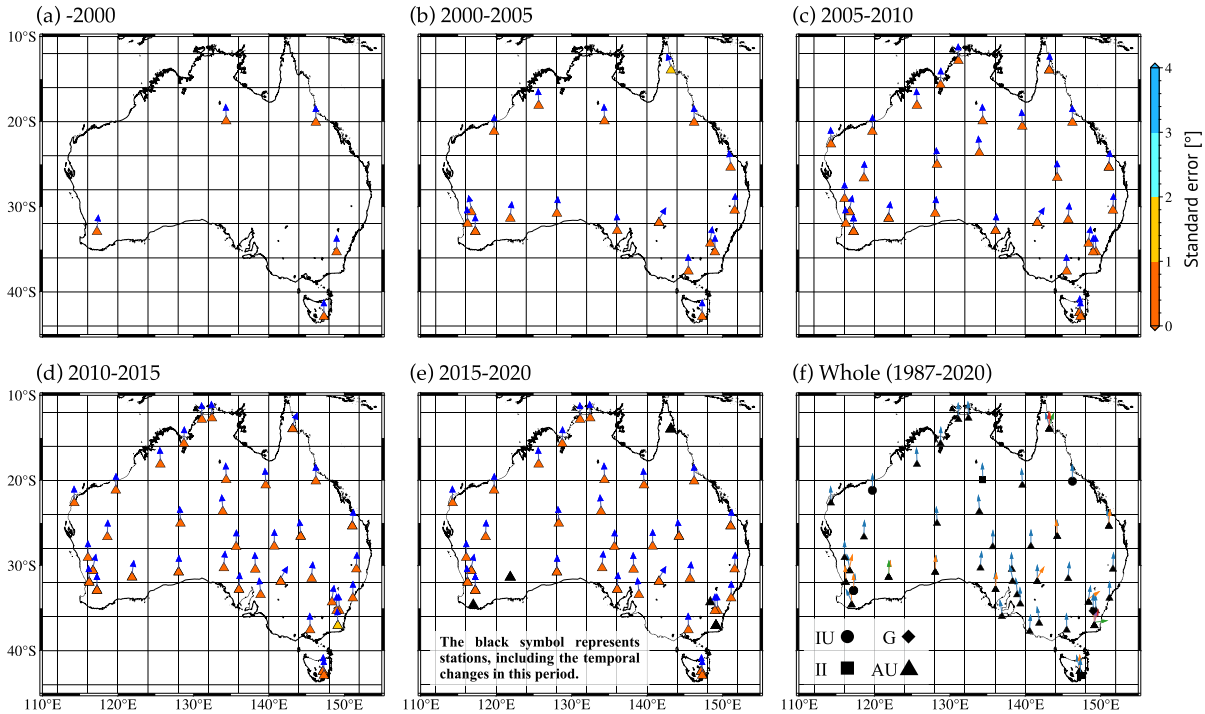


Figure 4

Map projections of horizontal misorientations from the geographic north for permanent seismic stations (II, IU, G, and AU) in Australia. **a**–**e** Arrows indicate the median directions of horizontal sensors over the designated period. Colors in the triangles indicate the estimated standard errors shown in the color bar on the right. Black triangles without arrows indicate stations with varying misorientations during the period. **f** A compiled map of estimated misorientations for the whole period of analysis. The colors of arrows indicate the horizontal sensor orientations in different periods. Black symbols indicate stations of different seismic networks

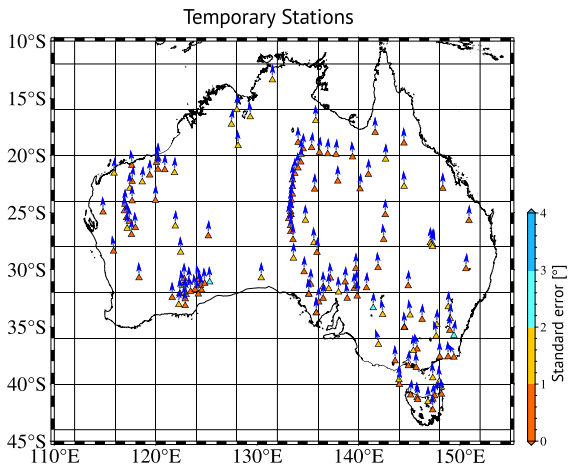


Figure 5

Station misorientations from the geographic north in a horizontal sensor for temporary seismic stations

Figure 3 shows a summary of P-wave polarization data (arrival-angle anomalies from the great-circle path for each event) for six permanent and two temporary stations during their operation periods until 2019. The horizontal-component channels of these stations have been labeled as BHN/BHE since their installation. At G.CAN (Canberra by GEOSCOPE; Fig. 3a), the station orientation estimated in this study is nearly 0° (Tables S1–S3 in Supplementary Materials), suggesting that this seismometer has been accurately aligned with the geographic north and east. AU.TOO (Fig. 3b) also shows no significant temporal changes, though our measurements suggest a slight misalignment (about $-1.2°$) from the north, which can be almost negligible. At AU.BBOO and AU.KMBL stations (Fig. 3c, d), we can see clear temporal changes in the trends of polarization angles, which coincide well with the timing of reported maintenance and/or instrument replacement. On the other hand, at AU.STKA and AU.COEN (Fig. 3e, f), unknown temporal changes in polarization angles are

Table 1

Comparison of recent misalignment measurements at AU stations by Eakin et al. (2023) and this study

Station	Eakin et al. (2023) (PKS and/or SKS)	This study (Teleseismic P-wave)
AU.ARPS	−6° (SKS)	−9.4° ±4.4° (2019; 6)
AU.FORT	0° (PKS), 3.5° (SKS)	4.4° ±0.4° (2003–2011; 69)
		1.4° ±0.2° (2011–2019; 404)
AU.HTT	−4° (PKS), −3° (SKS)	−6.3° ±0.2° (2010–2019; 399)
AU.KELC	−6° (SKS)	−9° ±1.3° (2019; 19)
AU.MGBR	−10° (SKS)	4.4° ±1.8° (2019; 30)
AU.MILA	6° (SKS)	1.7° ±0.6° (2011–2014; 44)
		−2.5° ±1.6° (2014–2016; 22)
		83° ±0.9° (2016–2018; 18)
		17° ±1.1° (2018–2019; 17)
		6.5° ±1.0° (2019; 12)
AU.MULG	6.6° (PKS and SKS)	5.0° ±0.4° (2013–2019; 219)
AU.SDAN	2.5° (SKS)	−1.5° ±0.7° (2018–2019; 48)
AU.STKA	31° (PKS and SKS)	−0.1° ±0.6° (2003; 23)
		31.0° ±0.2° (2003–2019; 899)
AU.YAPP	−13.4° (PKS and SKS)	−13° ±0.5° (2018–2019; 55)
AU.YNG	5° (PKS), 10° (SKS)	8.7° ±0.3° (2004–2017; 429)
		56° ±1.2° (2017–2019; 42)

Eakin et al. (2023) estimated these using PKS and/or SKS phases, as indicated. In the third column showing our results, the data period and the number of seismic events used are shown (e.g., 2011–2019; 100)

detected at unreported timings. In particular, STKA exhibits a very large misalignment of about 30° from north since the early stage of its operation.

Compiled maps of the estimated horizontal misorientations for permanent stations are displayed in Fig. 4, in which we show the misorientations in each period in Fig. 4a–e, and those compiled for the entire period of our analysis in Fig. 4f. For permanent stations, including those in the S1 network, the station misorientations and their standard errors are summarized in time-dependent horizontal bar graphs in Figs. S1, S2, and S5 in Supplementary Material 1 (hereafter SM1) and are separately tabulated in Tables S1 and S2 in Supplementary Material 2 (hereafter SM2). In particular, we can identify significant time-dependent variations of misorientations for AU stations. These temporal changes mostly coincide with the reported timing of maintenance and/or replacement by the EarthScope and AusPass. However, such temporal changes at several stations (e.g., AU.COEN) are found at unreported timings. The misorientation of some permanent stations from the geographic north is more than 10°, which may affect seismic waveform analysis, especially when using the horizontal components. Figure S6 (SM1) demonstrates the three-component seismograms observed at STKA to compare waveforms before and after correcting the station misorientations. In Fig. S6 (a) in SM1, we can see the apparent energy leakage of the P-wave from the radial to transverse component. In Sect. 4, we will discuss the effects of the station correction on azimuth-dependent receiver function analyses.

Some stations in AU exhibit relatively large standard errors compared to others (e.g., AU.ARPS; AU.MANU; see Fig. S1 and Table S1). These larger uncertainties may be influenced by the limited number of data samples and/or the back-azimuthal dependence of arrival angles.

For AU stations, we compare our measurements with those from a recent study in Table 1; we present our estimated misalignments for selected AU stations, along with PKS/SKS-based measurements from Eakin et al. (2023). We focused on stations for which Eakin et al. (2023) estimated non-zero misalignments, comparing them with the most recent misorientation data from our catalog between 1987 and 2019. Our measurements are generally in good agreement with those of Eakin et al. (2023). Note that

Table 2

Same as Table 1, but for selected temporary stations

Station	Eakin et al. (2023) (PKS and/or SKS)	This study (Teleseismic P-wave)
1E.SQA01	5° (SKS)	3.0° ±2.4° (2013–2014; 7)
1E.SQA09	10° (SKS)	16.0° ±1.4° (2013–2014; 7)
1E.SQA11	10° (SKS)	9.2° ±1.3° (2013–2014; 7)
1P.BA12	−25° (SKS)	−36.0° ±0.9° (2011–2013; 9)
1P.BA13	0° (SKS)	−1.8° ±0.8° (2011–2013; 26)
1P.BA19	9° (SKS)	−2.7° ±0.8° (2011–2013; 16)
7H.TB03	5° (SKS)	−3.0° ±1.0° (2011–2013)
7I.GA06	−5° (PKS), 0° (SKS)	−6.3° ±0.9° (2004; 7)
7I.GA08	−5° (SKS)	−3.4° ±0.9° (2004–2005; 10)
7I.TL10	−7° (PKS and SKS)	−6.1° ±0.8° (2003–2005; 19)
7I.TL14	0° (PKS), 8° (SKS)	−4.4° ±0.7° (2003–2005; 38)
7I.TL17	5° (SKS)	−1.4° ±0.4° (2003–2005; 30)
7K.SOC03	0° (PKS), 5° (SKS)	2.7° ±1.26° (2007–2008; 6)

large misalignment at AU.STKA is identical between both studies.

For another permanent network, S1 (Salmon et al., 2011), we obtained reliable misorientation estimates for only 13 stations. Although the use of the S1 network is outside the primary scope of our study, which focuses on the waveform analysis of high-quality broadband seismic records, we include the results for the S1 network in Figs. S5 and S8, Table S2, and Section S1.

3.2. Temporary Stations

The seismic records of temporary stations are generally less than two years long, and we could not find any significant temporal changes in the horizontal orientation. Figure 3g, h show examples of a time-dependent polarization measurement for selected temporary stations. As expected from the limited data acquisition period, we could not observe any significant temporal changes in the time-series data of these stations. In Fig. 5, we compiled the station orientation for all temporary stations that met the criteria described in Sect. 2. Also, we summarized the station orientations and their standard errors in Figs. S3 and S4 and Table S3 in Supplemental Materials. While some stations exhibit relatively large misalignments, the horizontal sensors at almost all temporary stations generally align with the geographic north and east directions (Fig. 5 and Fig. S3), suggesting proper installation. We also compare PKS/SKS-based measurements from Eakin et al. (2023) and teleseismic P-wave measurements from this study in Table 2, similar to the previous subsection. Overall, for most temporary stations, our results are generally consistent with those of Eakin et al. (2023). The discrepancies at some stations may be attributed to the utilized recording periods, the measurement quality for different seismic phases, and the number of employed events.

4. Discussion and Conclusions

In this section, we briefly examine the effect of the station correction on P-wave receiver function (P-RF) analysis. We computed the P-RFs at AU.STKA, where a large misorientation of over 30° was observed, and analyzed the differences between uncorrected and corrected P-RF data for both radial and transverse components. In these calculations, we considered the azimuthal dependence of P-RFs, which arises from the varying incoming directions (or back-azimuths) of teleseismic P-wave. The azimuth-dependent radial P-RFs reflect lateral variations in seismic discontinuities around the station (e.g., Kawakatsu et al., 2009; Kumar & Kawakatsu, 2011; Tonegawa et al., 2005). In addition, incorporating transverse P-RFs enables us to infer seismic

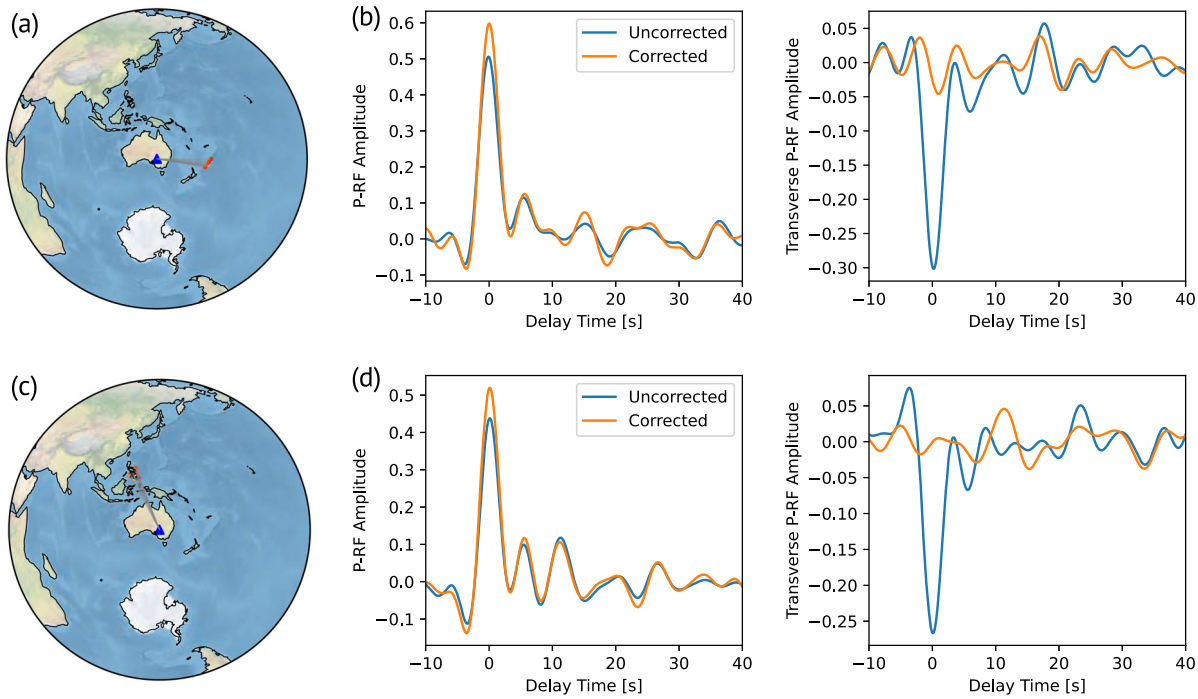


Figure 6
Comparison of P-wave receiver functions (P-RFs) for AU.STKA. **a**, **c** Maps showing event groups used for the P-RF analysis. **b** Stacked radial and transverse P-RFs for the eastern events shown in **a**. Blue and orange lines represent P-RFs from uncorrected and corrected teleseismic P-wave data, respectively. **d** Same as **b**, but for the northwestern events shown in **c**

anisotropy in the crust and upper mantle (e.g., Birkey & Ford, 2023; Park & Levin, 2016; Shiomi, 2017). Significant uncertainties in the horizontal component orientations could lead to misinterpretations in the results of P-RF analysis.

Figure S6 in Supplementary Material 1 shows an example of teleseismic P-wave records observed at AU.STKA before and after the correction for station orientation, clearly indicating the energy leakage of P-wave from radial to transverse in the uncorrected horizontal traces. Using these two sets of teleseismic P-wave data, we computed radial and transverse P-RFs for two incoming directions within narrow distance ranges (10°) (Fig. 6a, c). After calculating individual P-RFs, we selected P-RF traces using the cross-correlation coefficient (CC)-based selection method (Tkalcic et al., 2011), stacking all traces with CC $>$ 0.7. The resulting stacked P-RF traces are shown in Fig. 6b, d, and the stacking process is visually summarized in Figs. S8 and S9 in Supplementary Material 1. The radial P-RFs are generally consistent regardless of the correction of misorientation. Still, the relative amplitude of converted phases for the direct P-wave can be modulated, potentially affecting analyses that rely on RF amplitude. For the transverse RFs, clear differences emerge between the uncorrected and corrected P-RF traces. In the uncorrected transverse P-RFs, we can see clear signals of direct P-wave, Moho-converted phases, and their multiple reflections, contaminating the P-to-SH converted phases. This contamination prevents us from properly interpreting P-to-SH conversions, which can be generated by anisotropic properties or oblique interfaces. Therefore, proper corrections of station azimuths during the waveform processing are essential for the accurate interpretation of both radial and transverse P-RF amplitudes.

In this study, we constructed a comprehensive station orientation catalog for Australian broadband seismic stations by analyzing long-period teleseismic P-wave particle motion data. The catalog includes temporal variations in station misorientations. While

the timing of these changes is generally consistent with that reported in the EarthScope catalog, some stations exhibit changes at unexpected times. Finally, we assessed the utility of our catalog for receiver function analysis, demonstrating that correcting for station misorientation can significantly affect the amplitude analysis of RFs, particularly in the transverse component.

Acknowledgements

We thank Sima Mousavi and an anonymous reviewer for their thorough reviews, constructive suggestions, and insightful comments, which were very helpful in improving the original manuscript. All seismograms used in this study were obtained from the EarthScope Data Management Center (https://ds.iris.edu/ds/nodes/dmc/) and the Australian Passive Seismic Server (AusPass; https://auspass.edu.au/index.html). We used ObsPy (Beyreuther et al., 2010) for downloading and analyzing all seismic waveform data. We used matplotlib (Hunter, 2007), cartopy (Met Office, 2010), Generic Mapping Tools (Wessel et al., 2019), and PyGMT (Uieda et al., 2021) to create all figures.

Author Contributions KT: Conceptualization, Data curation, Methodology, Formal analysis, Funding acquisition, Investigation, Visualization, Software, Writing—Original draft; KY: Conceptualization, Data curation, Methodology, Funding acquisition, Investigation, Supervision, Project Administration, Writing—review and editing

Funding

This study was partly supported by JST SPRING grant number JPMJSP2119 to KT and JSPS KAKENHI (grant number 24KJ0294 to KT; 20K04096 and 23K03539 to KY).

Data Availability

The numerical data for our station misorientation catalog are included in PDF files provided as part of Supplementary Materials and Zenodo Repository (Tarumi & Yoshizawa, 2024). A sample Python script for the polarization analysis used in this study is also available from the same Zenodo repository (https://doi.org/10.5281/zenodo.16901548). All teleseismic waveform data used in this study are available from the EarthScope Data Management Center (https://ds.iris.edu/ds/nodes/dmc/) and the Australian Passive Seismic Server (AusPass; https://auspass.edu.au/index.html). The networks used in this study are: II (Scripps Institution of Oceanography, 1986); IU (Albuquerque Seismological Laboratory/USGS, 1988); G (Institut de physique du globe de Paris (IPGP) and École et Observatoire des Sciences de la Terre de Strasbourg (EOST), 1982); AU (Geoscience Australia, 2021); S1 (Salmon et al., 2011); 7B (Hilst & Kennett, 1993); 7D (Kennett, 1997); 7E (Kennett, 1998); 7F (Kennett et al., 1999); 7G (Kennet, 2000); 7H (Rawlinson & Kennett, 2001); 7I (Kennett, 2003); 7J (Reading & Kennett, 2005); 7K (Fontaine & Kennet, 2007); 6F (Rawlinson & Kennet, 2008); 1P (Reading & Rawlinson, 2011); 1E (Tkalcic et al., 2013b); 1K (Tkalcic et al., 2013a); 1G (Miller, 2014).

Declarations

Conflict of interest The authors declare no conflict of interest.

Publisher's Note Springer Nature remains neutral with regard to jurisdictional claims in published maps and institutional affiliations.

Springer Nature or its licensor (e.g. a society or other partner) holds exclusive rights to this article under a publishing agreement with the author(s) or other rightsholder(s); author self-archiving of the accepted manuscript version of this article is solely governed by the terms of such publishing agreement and applicable law.

References

Albuquerque, D. F., Rocha, M. P., Ianniruberto, M., et al. (2024). Estimating seismometer component orientation of the Brazilian seismographic network using teleseismic P-wave particle motion analysis and directional statistics. *Journal of South American Earth Sciences, 134*, Article 104754. https://doi.org/10.1016/j.jsames.2023.104754

Albuquerque Seismological Laboratory/USGS (1988). Global seismograph network (GSN-IRIS/USGS). https://doi.org/10.7914/SN/IU, https://www.fdsn.org/networks/detail/IU/

Beyreuther, M., Barsch, R., Krischer, L., et al. (2010). ObsPy: a Python toolbox for seismology. *Seismological Research Letters, 81*(3), 530–533. https://doi.org/10.1785/gssrl.81.3.530

Birkey, A., & Ford, H. A. (2023). Anisotropic structure of the Australian continent. *Frontiers in Earth Science, 10*, 1055480. https://doi.org/10.3389/feart.2022.1055480

Crampin, S. (1975). Distinctive particle motion of surface waves as a diagnostic of anisotropic layering. *Geophysical Journal of the Royal Astronomical Society, 40*(2), 177–186. https://doi.org/10.1111/j.1365-246x.1975.tb07045.x

Crampin, S., Stephen, R. A., & McGonigle, R. (1982). The polarization of P-waves in anisotropic media. *Geophysical Journal of the Royal Astronomical Society, 68*(2), 477–485. https://doi.org/10.1111/j.1365-246x.1982.tb04910.x

Deng, W., Han, G., Li, J., et al. (2024). Seismometer orientation measurements of broadband seismic stations in the China Digital Seismograph Network. *Bulletin of the Seismological Society of America*. https://doi.org/10.1785/0120240075

Dziewonski, A. M., Chou, T., & Woodhouse, J. H. (1981). Determination of earthquake source parameters from waveform data for studies of global and regional seismicity. *Journal of Geophysical Research: Solid Earth, 86*(B4), 2825–2852. https://doi.org/10.1029/jb086ib04p02825

Eakin, C. M., Davies, D. R., Ghelichkhan, S., et al. (2023). The influence of lithospheric thickness variations beneath Australia on seismic anisotropy and mantle flow. *Geochemistry, Geophysics, Geosystems, 24*(9). https://doi.org/10.1029/2023gc011066

Ekström, G. (2008). Polarization anomalies at various stations. https://www.ldeo.columbia.edu/~ekstrom/Projects/WQC/COMB_QC/

Ekström, G., & Busby, R. W. (2008). Measurements of seismometer orientation at USArray transportable array and backbone stations. *Seismological Research Letters, 79*(4), 554–561. https://doi.org/10.1785/gssrl.79.4.554

Ekström, G., Dalton, C. A., & Nettles, M. (2006). Observations of time-dependent errors in long-period instrument gain at global seismic stations. *Seismological Research Letters, 77*(1), 12–22. https://doi.org/10.1785/gssrl.77.1.12

Ekström, G., Nettles, M., & Dziewonski, A. (2012). The global CMT project 2004–2010: centroid-moment tensors for 13,017 earthquakes. *Physics of the Earth and Planetary Interiors, 200*, 1–9. https://doi.org/10.1016/j.pepi.2012.04.002

Fontaine, F. R., Barruol, G., Kennett, B. L. N., et al. (2009). Upper mantle anisotropy beneath Australia and Tahiti from P wave polarization: Implications for real-time earthquake location. *Journal of Geophysical Research: Solid Earth, 114*(B3). https://doi.org/10.1029/2008jb005709

Fontaine, F., & Kennet, B. (2007). SOC—Southern Craton. https://www.fdsn.org/networks/detail/7K_2007/

Geoscience Australia (2021). Australian national seismograph network data collection. https://doi.org/10.26186/144675, http://pid.geoscience.gov.au/dataset/ga/144675

Hejrani, B., & Tkalcic, H. (2020). Resolvability of the centroid-moment-tensors for shallow seismic sources and improvements from modeling high-frequency waveforms. *Journal of Geophysical Research: Solid Earth 125*(7). https://doi.org/10.1029/2020jb019643

van der Hilst, R., & Kennett, B. (1993). SKIPPY. https://www.fdsn.org/networks/detail/7B_1993/

van der Hilst, R., Kennett, B., Christie, D., et al. (1994). Project Skippy explores lithosphere and mantle beneath Australia. *Eos, Transactions American Geophysical Union, 75*(15), 177–181. https://doi.org/10.1029/94eo00857

Hunter, J. D. (2007). Matplotlib: A 2D graphics environment. *Computing in Science and Engineering, 9*(3), 90–95. https://doi.org/10.1109/mcse.2007.55

Institut de physique du globe de Paris (IPGP), École et Observatoire des Sciences de la Terre de Strasbourg (EOST) (1982). Geoscope, french global network of broad band seismic stations. https://doi.org/10.18715/GEOSCOPE.G, http://geoscope.ipgp.fr/networks/detail/G/

Kawakatsu, H., Kumar, P., Takei, Y., et al. (2009). Seismic evidence for sharp lithosphere-asthenosphere boundaries of oceanic plates. *Science, 324*(5926), 499–502. https://doi.org/10.1126/science.1169499

Kennett, B. (1997). KIMBA97. https://www.fdsn.org/networks/detail/7D_1997/

Kennett, B. (1998). KIMBA98. https://www.fdsn.org/networks/detail/7E_1998/

Kennet, B. (2000). West Australian Cratons. https://www.fdsn.org/networks/detail/7G_2000/

Kennett, B. (2003). TASMAL. https://www.fdsn.org/networks/detail/7I_2003/

Kennett, B., Debayle, E., & Gorbatov, A. (1999). QUOLL. https://www.fdsn.org/networks/detail/7F_1999/

Kennett, B. L. N., Fichtner, A., Fishwick, S., et al. (2013). Australian Seismological Reference Model (AuSREM): Mantle component. *Geophysical Journal International, 192*(2), 871–887. https://doi.org/10.1093/gji/ggs065http://gji.oxfordjournals.org/content/192/2/871.full.

Kennett, B. L. N., & Furumura, T. (2008). Stochastic waveguide in the lithosphere: Indonesian subduction zone to Australian craton. *Geophysical Journal International, 172*(1), 363–382. https://doi.org/10.1111/j.1365-246x.2007.03647.x

Kumar, P., & Kawakatsu, H. (2011). Imaging the seismic lithosphere-asthenosphere boundary of the oceanic plate. *Geochemistry, Geophysics, Geosystems, 12*(1). https://doi.org/10.1029/2010gc003358

Larson, E. W. F., & Ekström, G. (2002). Determining surface wave arrival angle anomalies. *Journal of Geophysical Research, 107*(B6). https://doi.org/10.1029/2000jb000048

Laske, G. (1995). Global observation of off-great-circle propagation of Long-Period surface waves. *Geophysical Journal International, 123*(1), 245–259. https://doi.org/10.1111/j.1365-246x.1995.tb06673.xhttp://gji.oxfordjournals.org/content/123/1/245.abstract.

Laske, G., & Masters, G. (1996). Constraints on global phase velocity maps from long-period polarization data. *Journal of Geophysical Research: Solid Earth, 101*(B7), 16059–16075. https://doi.org/10.1029/96jb00526

Met Office (2010). Cartopy: A cartographic python library with a Matplotlib interface. https://scitools.org.uk/cartopy

Miller, M. S. (2014). Transitions in the Banda Arc-Australia continental collision. https://www.fdsn.org/networks/detail/1G_2019/

Park, J., & Levin, V. (2016). Anisotropic shear zones revealed by backazimuthal harmonics of teleseismic receiver functions.

Geophysical Journal International, 207(2), 1216–1243. https://doi.org/10.1093/gji/ggw323

Rawlinson, N., & Kennett, B. (2001). TIGGER BB. https://www.fdsn.org/networks/detail/7H_2001/

Rawlinson, S., & Kennet, B. (2008). BILBY. https://www.fdsn.org/networks/detail/6F_2008/

Reading, A., & Kennett, B. (2005). CAPRA—Linkage. https://www.fdsn.org/networks/detail/7J_2005/

Reading, A., & Rawlinson, N. (2011). Bass Strait. https://www.fdsn.org/networks/detail/1P_2011/

Salmon, M., Balfour, N., & Sambridge, M. (2011) Australian Seismometers in Schools. https://www.fdsn.org/networks/detail/S1/

Schulte-Pelkum, V., Masters, G., & Shearer, P. M. (2001). Upper mantle anisotropy from long-period P polarization. *Journal of Geophysical Research: Solid Earth, 106*(B10), 21917–21934. https://doi.org/10.1029/2001jb000346

Scripps Institution of Oceanography (1986). Global seismograph network—IRIS/IDA. https://doi.org/10.7914/SN/II, https://www.fdsn.org/networks/detail/II/

Shiomi, K. (2017). Dissimilar receiver functions observed at very close stations in the Kii Peninsula, central Japan: Features and causes. *Earth, Planets and Space, 69*(1), 48. https://doi.org/10.1186/s40623-017-0631-5

Sun, W., Tkalcic, H., & Tang, Q. (2024). Single-station back-azimuth determination with the receiver function rotation technique validated by the locations of earthquakes, impacts, and explosions. *Seismological Research Letters*. https://doi.org/10.1785/0220240117

Tarumi, K., & Yoshizawa, K. (2024). Numerical Sheet for "Station-orientation catalog for Australian broadband seismic stations". https://doi.org/10.5281/zenodo.13985090

Tkalčić, H., Chen, Y., Liu, R., et al. (2011). Multistep modelling of teleseismic receiver functions combined with constraints from seismic tomography: Crustal structure beneath southeast China. *Geophysical Journal International, 187*(1), 303–326. https://doi.org/10.1111/j.1365-246x.2011.05132.x

Tkalčić, H., Kennett, B., Sippl, C., et al. (2013a). Albany-Fraser Experiment. https://www.fdsn.org/networks/detail/1K_2013/

Tkalčić, H., Kennett, B., Tanaka, S., et al. (2013b). Southern Queensland Spiral Array. https://www.fdsn.org/networks/detail/1E_2013/

Tonegawa, T., Hirahara, K., & Shibutani, T. (2005). Detailed structure of the upper mantle discontinuities around the Japan subduction zone imaged by receiver function analyses. *Earth, Planets and Space, 57*(1), 5–14. https://doi.org/10.1186/bf03351801

Uieda, L., Tian, D., Leong, W. J., et al. (2021). PyGMT: A Python interface for the Generic Mapping Tools. https://doi.org/10.5281/zenodo.5607255.

Vidale, J. E. (1986). Complex polarization analysis of particle motion. *Bulletin of the Seismological Society of America, 76*(5), 1393–1405. https://doi.org/10.1785/bssa0760051393

Wessel, P., Luis, J. F., Uieda, L., et al. (2019). The Generic Mapping Tools Version 6. *Geochemistry, Geophysics, Geosystems, 20*(11), 5556–5564. https://doi.org/10.1029/2019gc008515

Yoshizawa, K. (2014). Radially anisotropic 3-D shear wave structure of the Australian lithosphere and asthenosphere from multi-mode surface waves. *Physics of the Earth and Planetary Interiors, 235*, 33–48. https://doi.org/10.1016/j.pepi.2014.07.008http://www.sciencedirect.com/science/article/pii/S0031920114001745.

Yoshizawa, K., Yomogida, K., & Tsuboi, S. (1999). Resolving power of surface wave polarization data for higher-order heterogeneities. *Geophysical Journal International, 138*(1), 205–220. https://doi.org/10.1046/j.1365-246x.1999.00861.x

Zha, Y., Webb, S. C., & Menke, W. (2013). Determining the orientations of ocean bottom seismometers using ambient noise correlation. *Geophysical Research Letters, 40*(14), 3585–3590. https://doi.org/10.1002/grl.50698

(Received February 7, 2025, revised August 20, 2025, accepted August 28, 2025)